J Physiol 586.21 (2008) pp 5101–5118

The Journal of Physiology

The differential expression of low-threshold K^+ currents generates distinct firing patterns in different subtypes of adult mouse trigeminal ganglion neurones

Luigi Catacuzzeno[1], Bernard Fioretti[1,2], Daniela Pietrobon[2] and Fabio Franciolini[1]

[1] *Dipartimento di Biologia Cellulare e Ambientale, Universita' di Perugia, Perugia, Italy*
[2] *Dipartimento di Scienze Biomediche Sperimentali, Universita' di Padova, Padova, Italy*

In adult mouse trigeminal ganglion (TG) neurones we identified three neuronal subpopulations, defined in terms of their firing response to protracted depolarizations, namely MF neurones, characterized by a multiple tonic firing; DMF neurones, characterized by a delay before the beginning of repetitive firing; and SS neurones, characterized by a strongly adapting response. The three subpopulations also differed in several other properties important for defining their functional role *in vivo*, namely soma size, action potential (AP) shape and capsaicin sensitivity. MF neurones had small soma, markedly long AP and mostly responded to capsaicin, properties typical of a subgroup of C-type nociceptors. SS neurones had large soma, short AP duration and were mostly capsaicin insensitive, suggesting that most of them have functions other than nociception. DMF neurones were all capsaicin insensitive, had a small soma size and intermediate AP duration, making them functionally distinct from both MF and SS neurones. We investigated the ionic basis underlying the delay to the generation of the first AP of DMF neurones, and the strong adaptation of SS neurones. We found that the expression of a fast-inactivating, 4-AP- and CP-339,818-sensitive K^+ current (I_A) in DMF neurones plays a critical role in the generation of the delay, whereas a DTX-sensitive K^+ current (I_{DTX}) selectively expressed in SS neurones appeared to be determinant for their strong firing adaptation. A minimal theoretical model of TG neuronal excitability confirmed that I_A and I_{DTX} have properties congruent with their suggested role.

(Received 8 July 2008; accepted after revision 29 August 2008; first published online 4 September 2008)
Corresponding author F. Franciolini: Dipartimento Biologia Cellulare e Ambientale, Via Pascoli 1, I-06123 Perugia, Italy. Email: fabiolab@unipg.it

The trigeminal ganglion (TG) contains the cell bodies of a functionally heterogeneous population of neurones carrying a variety of sensory information originating from the head. These include mechanosensitive neurones originating from the muscles and joints, touch- and temperature-responding neurones originating from the skin, and nociceptive neurones originating from the face and deep tissues. In accordance with their functional heterogeneity, TG neurones have been found to differ in a number of morphological, biochemical and electrophysiological properties. It has been shown that some of these properties such as capsaicin sensitivity and AP duration (and to some extent soma size) associate with neurones displaying specific *in vivo* sensory functions (Lawson, 2002; Lazarov, 2002). The expression of the capsaicin-sensitive vanilloid (TRPV1) receptor selectively identifies a subpopulation of nociceptors (Caterina & Julius, 2001; Lawson *et al.* 2008). Electrophysiological studies have reported that wide action potentials, often characterized by an inflection during the repolarizing phase, are more probably found in putative TG and DRG nociceptors (Lawson, 2002; Connor *et al.* 2005).

The excitability and firing properties of TG neurones are aspects of greatest interest as they are the major determinants of the encoding capacity and transduction properties of the neurone. Heterogeneous firing properties have been reported in a number of studies on adult rat and mouse TG neurones. In particular, APs of different shape and duration have been described in TG neurones *in vitro* (Liu *et al.* 2001; Cabanes *et al.* 2002), and two different firing patterns in response to prolonged depolarizing stimuli have been reported, one characterized by a slowly adapting repetitive firing and the other by a rapidly adapting firing consisting of a single AP (Cabanes *et al.* 2002; Yoshida & Matsumoto, 2005; Yoshida *et al.* 2007). It remains unclear whether the different firing

DOI: 10.1113/jphysiol.2008.159384

patterns are associated with other specific cell features that may be important for defining the functional role of the neurones. Therefore, the first aim of this study was to identify the neuronal subpopulations present in adult mouse TG neurones defined in terms of their firing properties in response to long depolarizing pulses, and to establish a correlation between the different firing patterns and properties such as capsaicin sensitivity and AP shape and duration that, together with cell size, may distinguish between neurones belonging to different functional classes.

The second aim of our study was to characterize the ionic currents underlying some aspects of the different firing patterns displayed by adult mouse TG neurones. In fact, the ionic basis of the firing heterogeneity in TG neurones remains largely unknown. A low-threshold K^+ current having a high sensitivity to 4-AP has been found in a subpopulation of cold-insensitive, neonatal mouse TG neurones, and its activity has been proposed to limit excitability during cold stimulation (Viana *et al.* 2002). A dendrotoxin (DTX)-sensitive voltage-gated K^+ current has been shown to contribute to the rapid firing adaptation (single AP) of a subpopulation of TTX-resistant adult rat TG neurones of relatively small size (Yoshida & Matsumoto, 2005). Studies on adult mouse TG neurones are lacking, and one cannot extrapolate the findings in rat TG neurones given the large biochemical and functional differences reported for sensory neurones of the two species (Woodbury *et al.* 2004; Price & Flores, 2007).

Here we show that adult mouse TG neurones can be subdivided into three distinct subpopulations on the basis of their firing response to protracted depolarizing pulses: MF neurones showing multiple tonic firing, DMF neurones characterized by repetitive firing with a long delay, and rapidly adapting SS neurones with single AP firing. We demonstrate a strong correlation between MF firing, capsaicin sensitivity, small soma and long-duration AP with typical shoulder, as well as a strong correlation between DMF firing, capsaicin insensitivity, small soma and intermediate-duration AP with shoulder; SS firing was mostly found in capsaicin-insensitive neurones of larger size characterized by shorter AP duration (both with and without shoulder). We then investigated the ionic basis underlying some of the features of DMF and SS neurones, namely the delay to the first AP and the marked adaptation, respectively. We found that the selective expression of a fast-inactivating, 4-AP- and CP-339,818-sensitive K^+ current in DMF neurones participates in the generation of the delay to the first AP that characterizes this neuronal subpopulation, whereas a DTX-sensitive K^+ current selectively expressed in SS neurones appears to be determinant for the strong firing adaptation, hallmark of this neuronal subpopulation.

Methods

Cell culture

TG neurones were cultured from 30- to 40-day-old C57BL/6J mice using a previously described dissociation procedure (Liu & Simon, 1996). The animals were killed by cervical dislocation, following the Animal Experimentation guidelines of the University of Perugia. Trigeminal ganglia were dissected aseptically and collected in a HBSS solution containing (mM): NaCl 130, KCl 5, KH_2PO_4 0.3, $NaHCO_3$ 4, Na_2HPO_4 0.3 Hepes 10, glucose 10, pH 7.4 with NaOH. After about 30 min the ganglia were diced into small pieces and incubated for 40 min at 37°C in 1 mg ml^{-1} collagenase (Type XI-s, Sigma) in HBSS. Individual cells were dissociated by triturating the tissue through fire-polished glass pipettes having a progressively smaller tip diameter. The dissociated cells were then incubated for 10 min at 37°C in 0.5 mg ml^{-1} DNase I (type IV, Sigma), and further dissociated using Pasteur pipettes. After washing three times with DMEM medium (Gibco), the cells were cultured in DMEM supplemented with 10% fetal bovine serum, 100 IU ml^{-1} penicillin + 100 μg ml^{-1} streptomycin, plated on poly D-lysine-coated 35 mm Petri dishes, and cultured overnight at 37°C in a water-saturated atmosphere with 5% CO_2. Neurones were studied 12–24 h after plating. Only neurones without processes were used. Before electrophysiological recording, the cell body size was measured as the mean of the vertical and horizontal diameter using a micrometer eyepiece. All experiments were carried out at room temperature (20–25°C).

Electrophysiological recordings

Whole-cell, patch-clamp experiments under voltage-clamp and current-clamp configuration were performed with an EPC-10 amplifier (HEKA), using borosilicate pipettes with a resistance of 3–5 MΩ. Seventy per cent of the access resistance was actively compensated under voltage-clamp configuration. Only recordings having a residual access resistance lower than 10 MΩ were considered for further analysis. Current and voltage traces were sampled at 25 kHz and low-pass filtered at 3 kHz. Cell capacitance, membrane and access resistance were measured in voltage-clamp configuration at the beginning of the experiment (after about 2 min from the achievement of the whole-cell configuration) using the automatic compensation circuitry of the EPC-10 amplifier, at a holding potential of −60 mV. In experiments where the cell excitability was evaluated, after measuring the passive cell parameters, we switched to current-clamp mode and performed the following three protocols: (i) continuous recording of 1 min duration

with no applied currents, to allow electrical stabilization of the cell at the resting membrane potential; (ii) series of brief (1 ms) depolarizing current pulses from the resting potential, to evaluate the action potential shape; (iii) series of long (500 ms) depolarizing current pulses from the resting potential, to evaluate the multiple firing properties. Only cells showing a stable resting membrane potential during the application of the three protocols were considered for further analysis. Current-clamp experiments were performed using an intracellular solution containing (mM): KCl 135, $CaCl_2$ 1, $MgCl_2$ 2, EGTA-K 10, Hepes 10, NaATP 4, NaGTP 1, pH 7.2 with KOH, and an extracellular solution containing (mM): NaCl 145, KCl 5, $CaCl_2$ 2, $MgCl_2$ 1, Hepes 10, glucose 10, pH 7.4. In an earlier series of experiments, an internal solution lacking Na^+ was used, consisting of (mM): KCl 135, $CaCl_2$ 1, $MgCl_2$ 2, EGTA-K 10, Hepes 10, K_2-ATP 5, pH 7.2 with KOH. Recordings obtained with this solution were not used in the quantitative analysis of the excitability parameters. Recordings of K^+-selective currents were performed using a low potassium intracellular solution containing (mM): KCl 40, choline chloride 95, $CaCl_2$ 1, $MgCl_2$ 2, EGTA-K 10, Hepes 10, K_2ATP 5, pH 7.2 with KOH. The reduced intracellular K^+ allowed voltage-clamp recordings to be obtained with an estimated maximal voltage error lower than 10 mV. Following entry in the whole-cell configuration, the neurone was perfused with a Na^+-free, low-Ca^{2+} extracellular solution containing (mM): choline chloride 152, KOH 2, $CaCl_2$ 0.03, $Mg(OH)_2$ 3, Hepes 10, glucose 10, pH 7.4 with HCl.

In this study cell sampling was performed at random, and we recorded from neurones spanning the entire size range. Indeed, the distributions of soma diameters of the dissociated neurones used for electrophysiological studies and of neurones from TG slices stained with ematoxilin–eosin were largely overlapping (not shown). A partial exception is represented by the recordings aimed at investigation of I_{DTX}; in this case, we preferentially recorded from larger cells where the current of interest was most likely to be present. However, we always included in our sample neurones spanning the entire size range, to verify the differential expression of each current in neurones having different cell body size.

Materials

Capsaicin (Sigma) and CP-339,818 (Tocris Bioscience) were dissolved in DMSO stock solutions at concentrations of 1 mM and 10 mM, respectively. The final concentration of DMSO in the perfusing solution was never greater than 0.1%. We verified that this concentration of DMSO did not have significant effects on TG neurone excitability and K^+ currents. 4-Aminopyridine (4-AP, Sigma) tetraethylamonium (TEA, Sigma), dendrotoxin I (DTX-I, Alomone Laboratories), Heteropodatoxin II (HpTx, Alomone Laboratories) were dissolved in water as stock solutions at concentrations of 100 mM, 1 M, 100 μM and 100 μM, respectively.

Data analysis

The time course of the current, as well as kinetic and steady-state parameters, were fitted with the indicated equations by using the Simplex algorithm incorporated in Microcal Origin v. 4.1. The x^2 statistic was used as an indicator of the quality of the fit (Dempster, 1993). Unless otherwise indicated, x^2 values for the fits to the experimental data shown in the Results section correspond to levels of significance probability lower than 0.05 (the degrees of freedom being given by $n_{obs} - n_p$, where n_{obs} is the number of experimental points used in the fitting procedure, and n_p is the number of free parameters). A comparison of the X^2 values was used to ascertain the order of the Hodgkin–Huxley model (N) chosen to describe I_A and I_{DTX}. The number of exponential components necessary to fit the inactivation time courses was determined by comparing the sums of squares generated for the different fits, using the quantity $F = (S_f - S_g)\,(n - k_g)/(S_g\,k_f)$, where S_f, S_g, k_f and k_g are, respectively, the residual sum of squares, and number of parameters for each consecutive model (i.e. f and g), and n is the number of points in the dataset (see Dempster, 1993). The higher-order model g was accepted if the quantity F was higher than the value of the f-distribution with k_f and n-k_g degrees of freedom for a level of significance probability of 0.05.

Results are expressed as mean ± S.E.M. Statistical differences between means were analysed using the t test which does not assume equal variances. Where appropriate the significance level of probability (P) for the difference between mean values are given. In multiple comparisons, the t test was performed when the one-way ANOVA analysis detected a significant difference ($P < 0.05$).

Simulations

Simulations were performed with the XPPAUT software (http://www.math.pitt.edu/~bard/xpp/xpp.html) using a fourth-order Runge–Kutta algorithm with a time step (dt) of 0.04 ms. Variable and parameter units in the following equations are in the SI system. Voltage (V) was integrated according to the equation

$$\frac{dV}{dt} = \left(\frac{i_{COMM} - i_L - i_{DRK} - i_{TTXR} - i_{TTXS} - i_{Ca} - i_A - i_{DTX}}{C_m}\right),$$

where i_{COMM} is the command current, C_m is the cell electrical capacitance, set to 10 pF in the model neurone, and i_L, i_{DRK}, i_{TTXR}, i_{TTXS}, i_A and i_{DTX} are the leakage, K^+-selective DRK, Na^+-selective TTX-resistant, Na^+-selective TTX-sensitive, fast transient K^+-selective, and DTX-sensitive K^+-selective currents, respectively. i_L was described by the equation $i_L = 10^{-9}(V + 0.025)$, with parameters set to give, for the MF neurone model not expressing i_A and i_{DTX}, a membrane resistance and resting membrane potential well within the range experimentally observed in MF neurones. i_{DRK} and i_{TTXR} were modelled according to our experimental results obtained for these currents on small-diameter MF neurones (authors' unpublished observations). Specifically, i_{DRK} was described by the equation

$$i_{DRK} = 24 \times 10^{-9} m_{DRK}(V + 0.087)$$

where

$$\frac{dm_{DRK}}{dt} = \frac{(m^{\infty}_{DRK} - m_{DRK})}{\tau_{DRK}},$$

$$m^{\infty}_{DRK} = \left(1 + e^{-[(V+0.012)/0.008]}\right)^{-1}$$

and

$$\tau_{DRK} = \left[\left(0.0064 + 0.009e^{-V/0.01}\right)^{-1} + \left(0.02 + 71.6e^{V/0.005}\right)^{-1}\right]^{-1},$$

and i_{TTXR} was described by the equation

$$i_{TTXR} = 1.8 \times 10^{-7} m^3_{TTXR} h_{TTXR}(V - 0.068),$$

where

$$\frac{dm_{TTXR}}{dt} = \frac{(m^{\infty}_{TTXR} - m_{TTXR})}{\tau_{TTXR}},$$

$$m^{\infty}_{TTXR} = \left(1 + e^{-[(V+0.025)/0.006]}\right)^{-1},$$

$$\tau_{TTXR} = 0.0002 + 0.00085e^{-[(V+0.03)/0.023]^2},$$

$$\frac{dh_{TTXR}}{dt} = \frac{(h^{\infty}_{TTXR} - h_{TTXR})}{\tau h_{TTXR}},$$

$$h^{\infty}_{TTXR} = (1 + [(V + 0.04)/0.004])^{-1}$$

and

$$\tau h_{TTXR} = 0.0004 + 0.029e^{-[(V+0.038)/0.018]^2}$$

i_{TTXS} and i_{Ca} were modelled as described in Herzog *et al.* (2001) and Bertram & Behan (1999), respectively, with the maximal Ca^{2+} conductance set to 8 nS, a value in accordance with the HVA current density found in mouse TG neurones (Borgland *et al.* 2001). Finally, i_A and i_{DTX} were modelled based on the experimental results reported in this paper. Specifically, i_{DTX} was described by the equation

$$i_{DTX} = m^2_{DTX} h_{DTX} g_{DTX}(V + 0.087),$$

where

$$\frac{dm_{DTX}}{dt} = \frac{(m^{\infty}_{DTX} - m_{DTX})}{\tau_{DTX}},$$

$$m^{\infty}_{DTX} = \left(1 + e^{-[(V+0.064)/0.0086]}\right)^{-1},$$

$$\tau_{DTX} = 0.00125 + 0.00255e^{-[(V+0.07)/0.03]^2},$$

$$\frac{dh_{DTX}}{dt} = \frac{(h^{\infty}_{DTX} - h_{DTX})}{\tau h_{DTX}},$$

$$h^{\infty}_{DTX} = \left(1 + e^{[(V+0.042)/0.026]}\right)^{-1},$$

and

$$\tau_{DTX} = 0.0033 + 0.00339e^{-[(V+0.075)/0.0222]^2}.$$

i_A was described by the equation

$$i_A = m^3_A(a_i h_{1A} + (1 - a_i)h_{2A})g_A(V - E_K),$$

where

$$a_i = \left(1 + e^{[(V-0.01)/0.025]}\right)^{-1},$$

$$\frac{dm_A}{dt} = \frac{(m^{\infty}_A - m_A)}{\tau_A},$$

$$m^{\infty}_A = \left(1 + e^{-[(V+0.059)/0.019]}\right)^{-1},$$

$$\tau_A = 0.0055 + 0.00225e^{-[(V+0.09)/0.06]^2},$$

$$\frac{dh_{1A}}{dt} = \frac{(h^{\infty}_{1A} - h_{1A})}{\tau h_{1A}},$$

$$\frac{dh_{2A}}{dt} = \frac{(h^{\infty}_{2A} - h_{2A})}{0.128},$$

$$h^{\infty}_{1A} = h^{\infty}_{2A} = \left(1 + e^{[(V+0.081)/0.0127]}\right)^{-1}$$

and

$$\tau h_{1A} = 0.0022 + 0.002e^{-[(V+0.07)/0.042]^2}$$

g_{DTX} and g_A were set either to zero (to model the multiple firing response) or to values resulting in current densities within the range of our experimental estimations (see Fig. 3). Although the model shown in the Results section considered an electrical capacitance of 10 pF, a value close

to that observed for MF and DMF neurones, similar results were also obtained when the membrane capacitance was set to 35 pF (and all the conductances were appropriately scaled), a value close to the mean capacitance of SS neurones (data not shown).

Results

TG neurones show three distinct firing patterns

To assess the excitability properties of TG neurones, we made current-clamp recordings from 287 neurones using near-physiological ionic conditions. When 500-ms-long depolarizing current pulses were applied, three subpopulations of TG neurones were easily distinguished on the basis of the evoked firing pattern (Fig. 1*A*). Fifty four per cent ($n = 156$) responded with a repetitive firing (multiple-firing, MF, neurones), with 3.5 ± 0.3 APs elicited during 500-ms-long depolarizing stimuli at 2× the minimum stimulus amplitude needed to evoke an active response ($rheo_L$; $n = 39$; Fig. 1*C*). In 22% of the neurones ($n = 63$), the repetitive firing response was preceded by a delay (delayed multiple-firing, DMF, neurones), during which a graded depolarization is clearly visible. For a depolarizing stimulus to 2× the $rheo_L$, the mean delay to the first AP amounts to 64 ± 10 ms ($n = 25$), a value more than 6 times greater than that observed in MF neurones (10.4 ± 4.8 ms, $n = 39$). This delay tended to decrease in duration with higher injected currents (Fig. 1*B*), and usually disappeared with injected currents higher than 3× the $rheo_L$ (data not shown). DMF neurones also differed from MF neurones in firing frequency (for an injected current of 2× the $rheo_L$ the number of spikes elicited during the pulse amounted to 5.4 ± 0.5, $n = 25$, a value significantly higher than that found for MF neurones, $P < 0.05$; Fig. 1*C*). The remaining neurones (24%; $n = 68$) showed a strongly adapting response, and fired only a single action potential (single-spiking, SS, neurones) regardless of the amount of the current injected (tested with depolarizing currents of at least 25 pA pF^{-1}; Fig. 1*A*).

Quantitative analysis in neurones showing a stable resting membrane potential throughout the recording (39 MF, 25 DMF and 19 SS neurones) revealed that the three subpopulations also differed in other passive and active electrophysiological properties (Fig. 2*B*

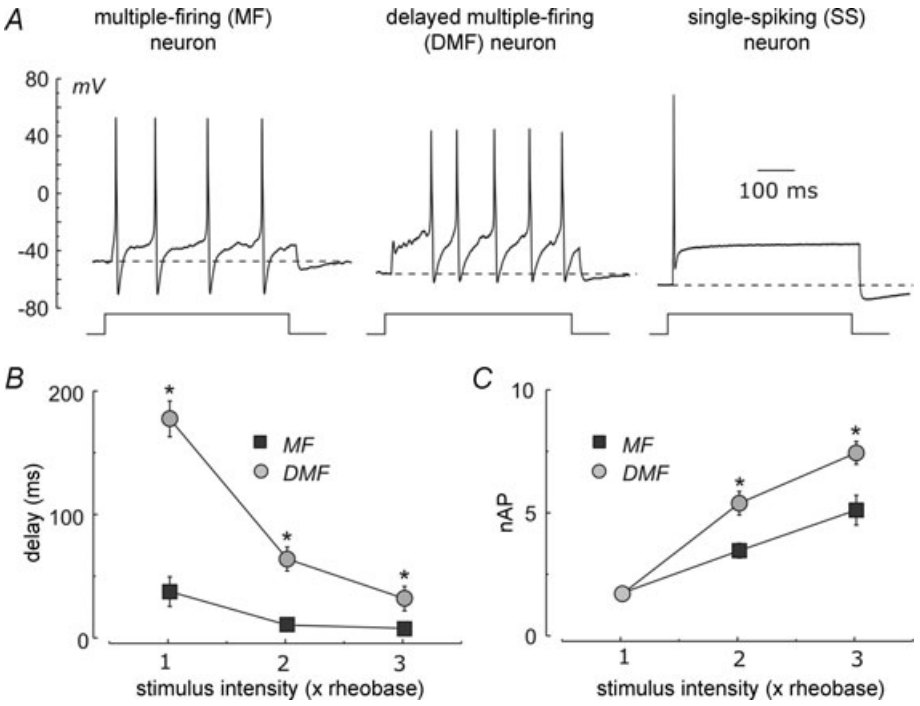

Figure 1. Mouse TG neurones can be classified into three distinct populations displaying different firing patterns
A, representative voltage responses recorded under current-clamp mode in response to 500 ms depolarizing pulses from the three different TG neurone subpopulations. The depolarizing current stimulus was 2 times the rheobase of the neurone under study. *B* and *C*, plots of the duration of the delay to the first action potential and the mean number of evoked AP in 39 MF and 25 DMF neurones as a function of the stimulus amplitude. The stimulus amplitude is expressed in units of the rheobase measured by applying 500-ms-long depolarizing pulses ($rheo_L$). Data were obtained from voltage responses to depolarizing pulses 500 ms long (cf. *A*). Asterisks indicate significant differences between MF and DMF neurones ($P < 0.05$).

and Table 1). All passive and active parameters analysed were significantly different between MF and SS neurones and, with the exception of the rheobase measured using short (1 ms) depolarizing pulses ($rheo_S$), between DMF and SS neurones. In particular, SS neurones had more negative resting potentials, shorter duration action potentials and smaller amplitude AHPs than MF and DMF neurones (the latter having

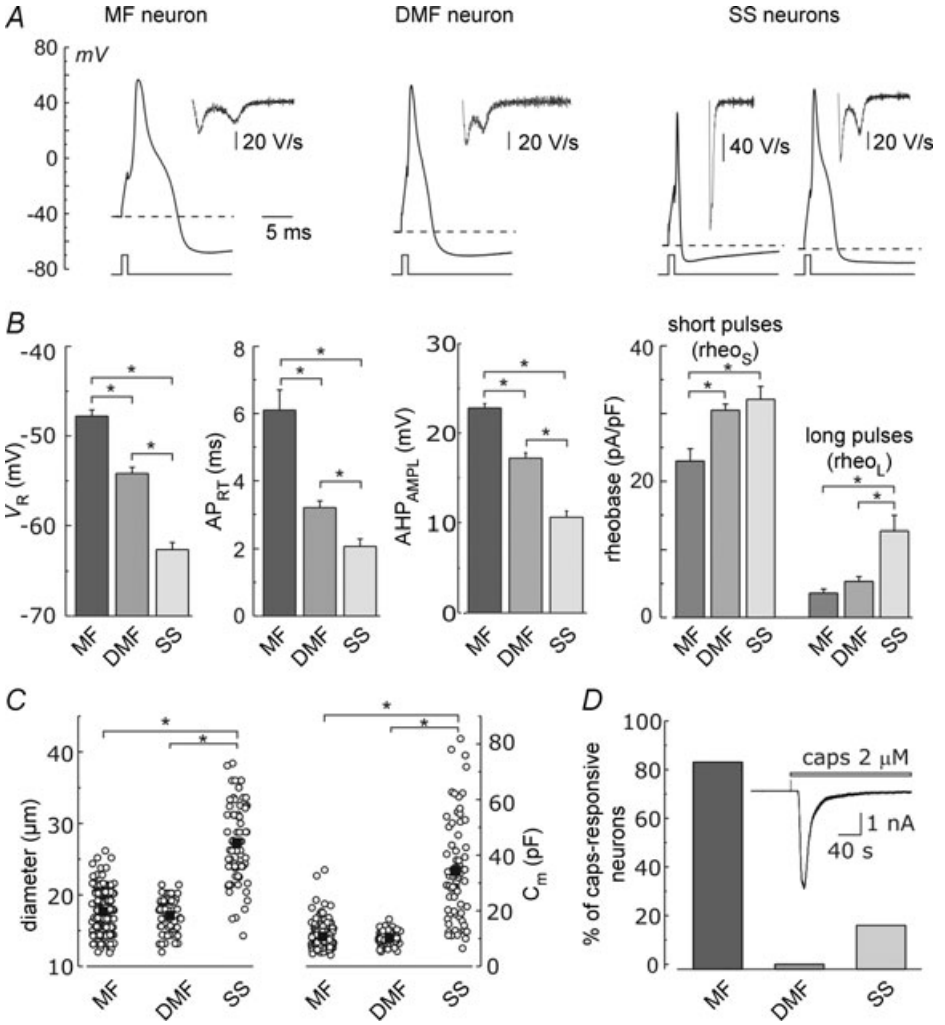

Figure 2. Differences in AP shape, cell size and capsaicin responsiveness of the three TG neuronal populations

A, voltage traces obtained in response to a 1-ms-long depolarizing current pulse in an MF neurone, a DMF neurone and two SS neurones differing for the presence of a shoulder during the repolarizing phase of the AP. Insets: time derivative of the corresponding voltage traces taken during the repolarizing phase of the action potential. *B*, comparison of several electrophysiological parameters assessed in 39 MF, 25 DMF and 17 SS neurones stimulated with the protocol shown in *A*: resting potential (V_R), AP repolarizing time (AP_{RT}), rheobase obtained by stimulating with short (1 ms, $rheo_S$) and long (500 ms, $rheo_L$) depolarizing currents, and voltage amplitude of the after-hyperpolarization (AHP_{ampl}). Data are given as mean ± S.E.M., and significant differences ($P < 0.05$) are marked by an asterisk. Two SS neurones, having an AP_{RT} value considerably larger than the remaining population (7.1 and 8.8 ms), were discarded from the analysis (outliers according to the Grubb's test). If these two neurones were considered, the mean AP_{RT} of DMF and SS neurones resulted in being not significantly different ($P > 0.05$). *C*, bar plots showing the soma diameter and electrical capacitance resulting from 156 MF, 63 DMF and 68 SS neurones. Filled squared symbol represent the mean ± S.E.M. for the diameter and capacitance of the three subpopulations. Asterisks indicate significant differences. *D*, bar plot showing the percentage of MF, DMF and SS neurones that were found to respond with a detectable (> 10 pA) inward current (at −60 mV of applied potential) following capsaicin (2 μM) application to the external solution. Capsaicin was applied on 71 MF, 33 DMF and 25 SS neurones. Inset: typical current response of an MF neurone to bath application of 2 μM capsaicin. The holding potential was −60 mV.

Table 1. AP parameters assessed on the three TG neuronal populations

Parameter	MF neurones Value ± S.E.M. (*n*)	DMF neurones Value ± S.E.M. (*n*)	SS neurones Value ± S.E.M. (*n*)	*P* (MF *versus* DMF)	*P* (MF *versus* SS)	*P* (DMF *versus* SS)
C_m (pF)	10.1 ± 0.5 (39)	10.6 ± 0.4 (25)	39.3 ± 5.8 (17)	0.5	**5.2e^{-10}**	**4.9e^{-7}**
V_r (mV)	−47.8 ± 0.7 (39)	−54.2 ± 0.7 (25)	−62.7 ± 0.8 (17)	**2.5e^{-7}**	**7.4e^{-17}**	**3.4e^{-9}**
AP_{ampl} (mV)	102.1 ± 0.7 (39)	101.6 ± 1.0 (25)	118 ± 2 (17)	0.66	**8e^{-12}**	**7.6e^{-9}**
AP_{rt} (ms)	6.1 ± 0.6 (39)	3.2 ± 0.2 (25)	2.1 ± 0.2 (17)	**7.5e^{-4}**	**1.5e^{-4}**	**5e^{-4}**
AHP_{ampl} (mV)	22.8 ± 0.5 (39)	17.2 ± 0.6 (25)	10.6 ± 0.7 (17)	**4.9e^{-10}**	**8.9e^{-20}**	**3.6e^{-9}**
AHP_{dur} (ms)	33.4 ± 2.8 (39)	31.4 ± 2.7 (25)	68.4 ± 14.4 (17)	0.63	**0.001**	**0.004**
r_d (V s^{-1})	157 ± 9 (39)	153 ± 9 (25)	538 ± 46 (17)	0.75	**4.5e^{-16}**	**3e^{-12}**
r_{r1} (V s^{-1})	−48.0 ± 3.3 (39)	−62.7 ± 3.1 (25)	−138 ± 20 (17)	**0.003**	**4.3e^{-8}**	**7.2e^{-5}**
r_{r2} (V s^{-1})	−37.9 ± 2.1 (39)	−38.8 ± 1.9 (25)	−71.1 ± 8.9 (14)	0.75	**2.8e^{-6}**	**5.4e^{-5}**
t_r (ms)	5.2 ± 0.6 (39)	2.3 ± 0.1 (25)	1.5 ± 0.2 (14)	**3.6e^{-4}**	**7.6e^{-4}**	**0.004**
$rheo_S$ (pA pF^{-1})	23.0 ± 1.8 (39)	30.5 ± 0.9 (25)	32.1 ± 1.9 (17)	**0.002**	**0.004**	0.4
$rheo_L$ (pA pF^{-1})	3.59 ± 0.62 (39)	5.32 ± 0.71 (25)	12.9 ± 2.3 (17)	0.077	**5.6e^{-10}**	**1.8e^{-6}**
R_i (GΩ)	1.20 ± 0.06 (39)	0.80 ± 0.04 (25)	0.36 ± 0.05 (17)	**1.6e^{-5}**	**1.8e^{-11}**	**4.2e^{-8}**

The parameters considered are: Cm, membrane capacitance V_r, resting membrane potential; AP_{ampl}, AP amplitude; AP_{rt}, AP repolarizing time; AHP_{ampl}, amplitude of the after-hyperpolarization; AHP_{dur}, duration of the after-hyperpolarization at half amplitude; r_d, maximal rate of depolarization; r_{r1}, first maximal rate of repolarization; r_{r2}, second maximal rate of repolarization; t_r, time between the two maximal rate of repolarization; $rheo_S$, minimum injected current (of 1 ms duration) that triggers an AP; $rheo_L$, minimum injected current (of 500 ms duration) that triggers an AP; R_i, input resistance, assessed in voltage-clamp mode by applying repolarizing pulses from −60 to −80 mV. The last three columns report the significance level assessed by a *t* test performed on MF *versus* DMF, MF *versus* SS, and DMF *versus* SS neurones. *P* values lower than 0.05 are in bold.

intermediate values between those of MF and SS neurones; Table 1). As shown in Fig. 2*A*, while most MF and DMF neurones displayed a characteristic shoulder during the repolarizing phase of the action potential (evident as a double minimum in the voltage rate of repolarization; see inset to Fig. 2*A*), SS neurones could be clearly divided into two subpopulations differing for the presence (16/19) or absence (3/19) of the shoulder.

We then verified whether the three neuronal subpopulations differed in other parameters that could give clues to their functional properties. As shown in Fig. 2*C*, MF and DMF neurones had similar small cell diameter ($17.7 \pm 0.2\ \mu$m, $n = 156$ and $17.1 \pm 0.3\ \mu$m, $n = 63$) and capacitance (10.7 ± 0.4 pF, $n = 156$ and 10.3 ± 0.3 pF, $n = 63$), while SS neurones had a significantly higher soma size, with mean diameter and capacitance of $27.2 \pm 0.7\ \mu$m and 34.3 ± 2.2 pF ($n = 68$, $P < 0.05$), respectively. We then assessed whether the three neuronal subpopulations responded to the TRPV1 agonist capsaicin since this response identifies a subpopulation of sensory neurones carrying nociceptive information (Caterina & Julius, 2001). As shown in the plot of Fig. 2*D*, we found that the majority of MF neurones tested (59 out of 71) were capsaicin responsive, while none of the DMF neurones tested (33) and only few (4 out of 25) SS neurones were able to respond to capsaicin with a detectable (> 10 pA) inward current. Taken together, these data show that the three neuronal subpopulations identified on the basis of the evoked firing pattern strongly correlate with distinct markers of sensory function.

Ionic basis of the heterogeneity in the evoked firing response

To understand the ionic basis of the different firing patterns found in the three neuronal subpopulations, we looked for differences in the ionic currents recorded under physiological conditions. In recordings from 141 cells, we first identified the neurone as MF, DMF or SS by looking at its firing response under current-clamp mode; then we went to voltage-clamp to record the macroscopic currents evoked by depolarizing voltage pulses. As shown in Fig. 3, a striking difference could easily be discerned in the amount and kinetics of the outward currents evoked by small depolarizing pulses. The large majority of MF neurones (89/95) responded to a −40 mV depolarizing step with a low amplitude, slowly activating outward current; in contrast, DMF neurones always responded with a prominent fast transient outward current (24/24), and SS neurones responded with a sustained outward current that activated much faster and had a much higher amplitude than that of MF neurones (22/22). To this general rule, we found only few exceptions, consisting of a small number of MF neurones (6/95) displaying a significant fast transient outward current similar to that found in DMF neurones. Figure 3*B* shows a quantitative estimate of the peak and sustained current amplitude, and the activation kinetics of the outward current performed on a subgroup of these recordings selected for having a maximal voltage error due to series resistance lower than 10 mV.

The fast-inactivating, low threshold outward current of DMF neurones. The consistent observation of a fast transient outward current in DMF neurones suggested that the presence of A-type Kv currents (I_A) could be mainly responsible for the initial delay in spike onset characterizing their firing, as found in other types of neurones (Kanold & Manis, 1999, 2005; Shibata *et al.* 2000; Vydyanathan *et al.* 2005).

Indeed, recordings with intra- and extracellular solutions chosen to isolate K^+ currents (see Methods), revealed in a subpopulation of neurones a fast-inactivating transient K^+ current, having properties similar to those described for I_A in other sensory neurones (Gold *et al.* 1996; Winkelman *et al.* 2005). I_A was isolated from the remaining sustained current as the difference between currents evoked following two different pre-pulse potentials (−40 mV and −110 mV; Fig. 4*A*). The I_A current displayed partially overlapping activation and inactivation curves (Fig. 4*B*), giving rise to a small but significant window current near the resting membrane potential of DMF neurones (cf. with Table 1). Application of a standard two-pulse protocol with a variable inter-pulse at −100 mV for studying recovery from inactivation (inset to Fig. 4*C*) revealed that the major component of the I_A (> 90%) recovered from inactivation with fast kinetics ($\tau = 41$ ms), while the remaining portion did it more slowly ($\tau = 899$ ms; Fig. 4*C*). In agreement with the conclusion that the I_A characterized in Fig. 4 accounts for the fast transient outward current almost selectively observed in DMF neurones under physiological conditions, I_A was selectively observed in a subpopulation of small sized TG neurones (Fig. 4*D*, left), having a mean capacitance of 11.9 ± 1.4 pF ($n = 29$), a value not significantly different from the mean capacitance found for DMF neurones (10.6 ± 0.3 pF, $n = 63$; $P > 0.05$). In addition I_A strongly correlated with the unresponsiveness to capsaicin (Fig. 4*D*, right), as is the case for DMF neurones (see Fig. 2).

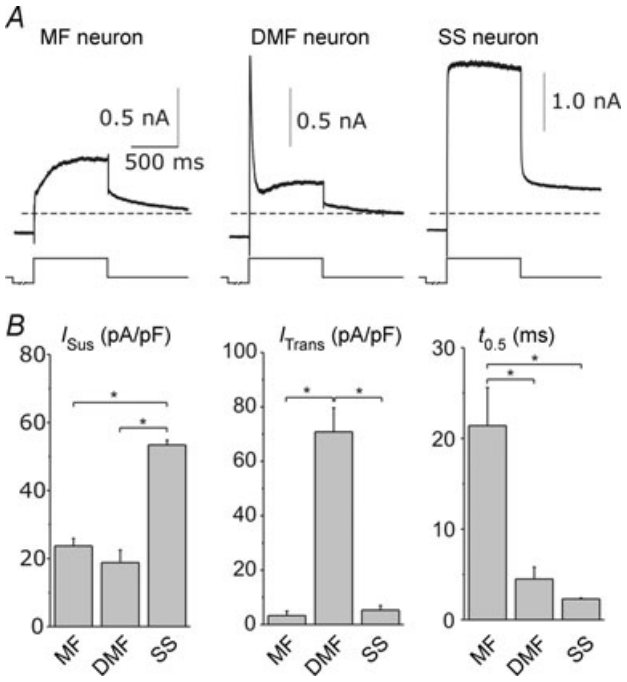

Figure 3. The three TG neuronal populations differ for the functional expression of low-threshold outward currents
A, typical current responses obtained from the three TG neuronal populations by applying a depolarizing pulse to −40 mV preceded by a 1.5 s conditioning step to −110 mV. Note the different scale bar for the SS neurone, and for the MF and DMF neurones. *B*, mean sustained and transient current densities, and time of half-maximal activation obtained for 37 MF neurones, 18 DMF neurones and 12 SS neurones, using current responses similar to that shown in *A*. Asterisks indicate significant differences.

Fast-inactivating, A-type currents can be produced by members of the *Shaker* (Kv1.4), *Shaw* (Kv3.3 and Kv3.4), and *Shal* (Kv4.1, 4.2 and 4.3) subfamilies of Kv channels. Since the currents sustained by these subunits differ markedly in their pharmacological properties (Gutman *et al.* 2005), to gain clues on the subunit composition of the I_A expressed in DMF TG neurones we tested its sensitivity to different drugs. I_A was effectively inhibited by millimolar concentrations of the classical I_A blocker 4-AP (Fig. 5*A* and *B*), that also significantly inhibited the transient outward current evoked in DMF neurones under physiological conditions ($n = 3$, data not shown). I_A was instead insensitive to 1 mM TEA, a selective blocker of transient currents sustained by Kv3 subunits (Coetzee *et al.* 1999; Pérez-García *et al.* 2004), and 100 nM DTX-I, a selective blocker of Kv1.1, Kv1.2 and Kv1.6, that blocks a slowly inactivating low-threshold K^+ current in a variety of neurones (Harvey & Robertson, 2004; Fig. 5*A* and *B*). We also verified the sensitivity of I_A to the Kv4-specific inhibitor heteropodatoxin (HpTx; Sanguinetti *et al.* 1997; Zarayskiy *et al.* 2005) and to CP-339,818, an effective inhibitor of Kv1.4 channels (Nguyen *et al.* 1996). HpTx at 500 nM was totally ineffective in blocking this current (Fig. 5*A* and *B*), while a significant inhibition could be achieved using 1 and 3 μM CP-339,818. However, CP-339,818 also partially blocked a sustained K^+ current component (see Fig. 5*A*), suggesting that its action is not fully selective for I_A.

Since the I_A described above has properties congruent with the generation of a delay to the first action potential (Kanold & Manis, 1999), we looked at the effects of the I_A blockers 4-AP and CP-339,818 on the delay of DMF neurones. As shown in Fig. 6, bath application of 1 mM 4-AP, which inhibits about 40% of the I_A (see Fig. 5), completely suppressed the delay to the first action potential, indicating a critical role of I_A in setting the firing pattern of DMF neurones. In addition to eliminating the delay, 4-AP also induced a marked increase in the duration of the AP, and a significant membrane depolarization as well as an increase in spike frequency (Fig. 6*B*). Similarly

we found that 3 μM CP-339,818 was able to drastically reduce the delay to the first AP (Fig. 6*A* and *B*). CP-339,818 also depolarized the resting membrane potential, but to a lesser extent than 4-AP (Fig. 6*A* and *B*). In contrast to what we observed with 4-AP, CP-339,818 did not increase the AP duration and did not change spike frequency (Fig. 6*A* and *B*).

To test for the contribution of the 4-AP and CP-339,818-induced membrane depolarization to the removal of the delay to the first AP (as a consequence of an increased steady-state inactivation of I_A), in three neurones we imposed a negative holding current to reset the resting membrane potential to the value observed before the pharmacological treatment that eliminated the delay. In two of the three neurones tested with 1 mM 4-AP we observed the reappearance of a delay which, however, had a duration about half that observed in control conditions, and completely disappeared upon bath application of 3 mM 4-AP (data not shown). In none of the three neurones tested with CP-339,818 did the same

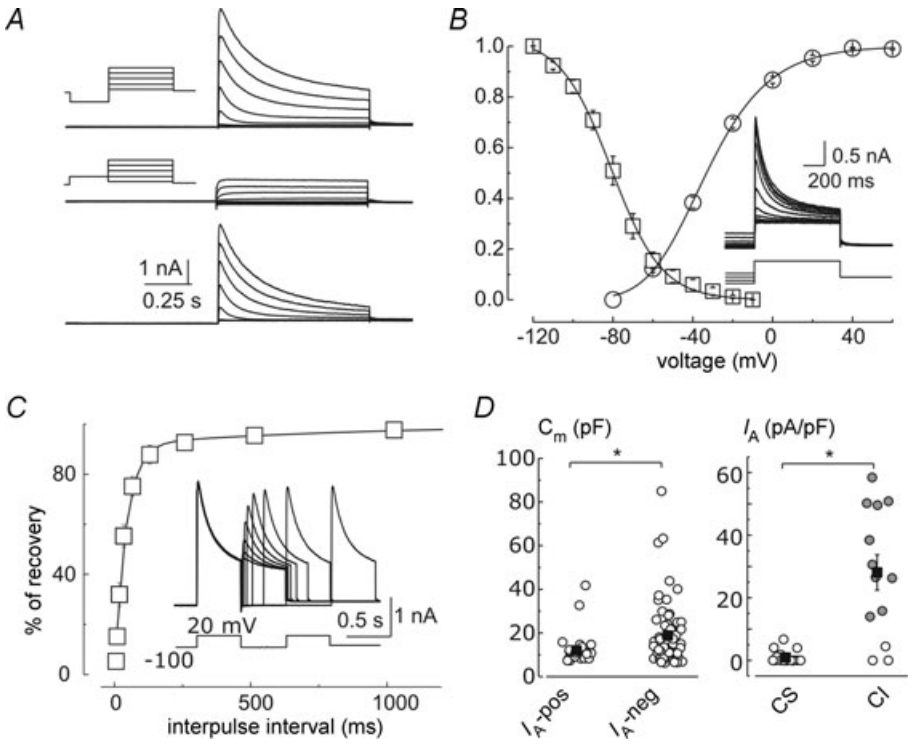

Figure 4. Biophysical and molecular properties of I_A
A, current traces obtained from a small TG neurone expressing a prominent I_A, in response to depolarizing pulses from −120 to +20 mV in 20 mV steps. The depolarizing stimuli were preceded by a 1.5 s conditioning prepulse to either −110 mV (upper panel) or −40 mV (middle panel). The current traces at the bottom panel represent a point-by-point subtraction of the current traces obtained with the two different conditioning prepulses. *B*, plot showing the mean steady-state activation ($n = 7$) and inactivation ($n = 6$) of the I_A. Steady-state activation data were assessed from the peak conductance of I_A, isolated as shown in *A*. Steady-state inactivation was assessed from the peak current obtained at +20 mV after conditioning the neurone at varying membrane potentials for 1.5 s, as shown for a typical experiment in the inset. Activation and inactivation data points were fitted with a third power Boltzmann and Boltzmann relationships, respectively (continuous curves), giving $V_{1/2}$ of −59.9 and −80.9 mV, and k of 19.1 and −12.7 mV, respectively. *C*, plot of the mean fractional recovery of the I_A *versus* the duration of the conditioning pulse, assessed from four TG neurones by applying the experimental protocol shown. The continuous line represents the best fit of the experimental data with the relationship:% recovery $= a_1 (1 - e^{-t/\tau 1}) + (1 - a_1)(1 - e^{-t/\tau 2})$, with $a_1 = 92$, $\tau_1 = 41$ ms and $\tau_2 = 899$ ms. Inset: current traces obtained by applying two depolarizing pulses to +20 mV separated by a conditioning pulse to −100 mV of variable duration. *D*, left: plots of membrane capacitance of cells expressing or not expressing a detectable transient K^+ current (greater than 10 pA pF^{-1} at −40 mV) with an inactivation kinetics compatible with the I_A shown in *A*. Open symbols represent individual TG neurones ($n = 80$), and closed symbols represent mean cell capacitances, that were found to differ significantly between neurones expressing and not expressing I_A. Right: plot of the I_A density in cells found to be capsaicin sensitive or capsaicin insensitive. Open symbols represent individual TG neurones ($n = 32$), and filled symbols represent mean current densities, that were found to differ significantly between capsaicin-sensitive or capsaicin-insensitive neurones. Asterisks indicate significant differences.

manoeuver induce the reappearance of a significant delay (data not shown; see higher fractional block of I_A by 3 μM CP-339,818 with respect to that obtained with 1 mM 4-AP in Fig. 5). Although not fully specific for I_A, the ability of both 4-AP and CP-339,818 to eliminate the delay to the first AP is consistent with the conclusion that this current plays a key role in determining the delayed firing typical of DMF neurones.

The low-threshold outward current of SS neurones. The selective expression of a low-threshold fast-activating sustained outward current in SS neurones (see Fig. 3) suggested the hypothesis that the presence of DTX-I-sensitive low-threshold Kv currents (I_{DTX}) could be mainly responsible for the strongly adapting behaviour of this TG subpopulation, as shown in rat TG neurones and other types of neurones (Glazebrook *et al.* 2002; Mo *et al.* 2002; Dodson *et al.* 2002; Barnes-Davies *et al.* 2004; Yoshida & Matsumoto, 2005). To test this hypothesis, we investigated the biophysical and pharmacological properties of the low-threshold K^+ current that was selectively detected in large TG neurones (Fig. 7*C*), probably representing SS neurones (see Figs 2 and 3). In these neurones, a fast-activating K^+ current with an activation threshold as low as −60 mV could be blocked by the Kv1.1, Kv1.2 and Kv1.6 selective inhibitor DTX-I (100 nM), leaving unaltered an underlying slowly activating, high-threshold current (Fig. 7*A*). The DTX-sensitive current (I_{DTX}), isolated by subtraction of the current traces in control conditions and in the presence of DTX-I (Fig. 7*A*, third panel), showed a strongly voltage-dependent inactivation rate (in contrast to the inactivation properties of I_A; see Fig. 4). The marked voltage-dependent inactivation of this current is consistent with and explains the sustained time course of the outward current at −40 mV in large-diameter SS neurones recorded under physiological conditions (see Fig. 3). The mean DTX-sensitive current density at −40 mV was 30.8 ± 5.4 pA pF^{-1} ($n = 20$).

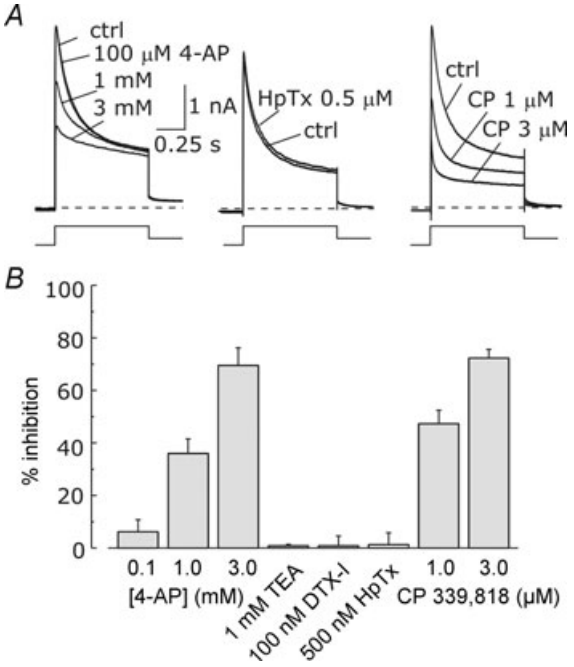

Figure 5. Pharmacological properties of I_A
A, current traces showing the effect of 0.1, 1 and 3 mM 4-AP, 500 nM HpTx and 1 and 3 μM CP-339,818 on the current evoked by applying depolarizing pulses to +20 mV preceded by a 1.5 s conditioning pulse to −110 mV. *B*, bar plot showing the mean percentage inhibition of the transient component of the outward current (peak minus sustained current) following application of 0.1 mM ($n = 6$), 1 mM ($n = 5$) and 3 mM ($n = 4$) 4-AP, 100 nM DTX-I ($n = 2$), 1 mM TEA ($n = 2$), 500 nM HpTx ($n = 5$), and 1 ($n = 5$) and 3 μM ($n = 4$) CP-339,818.

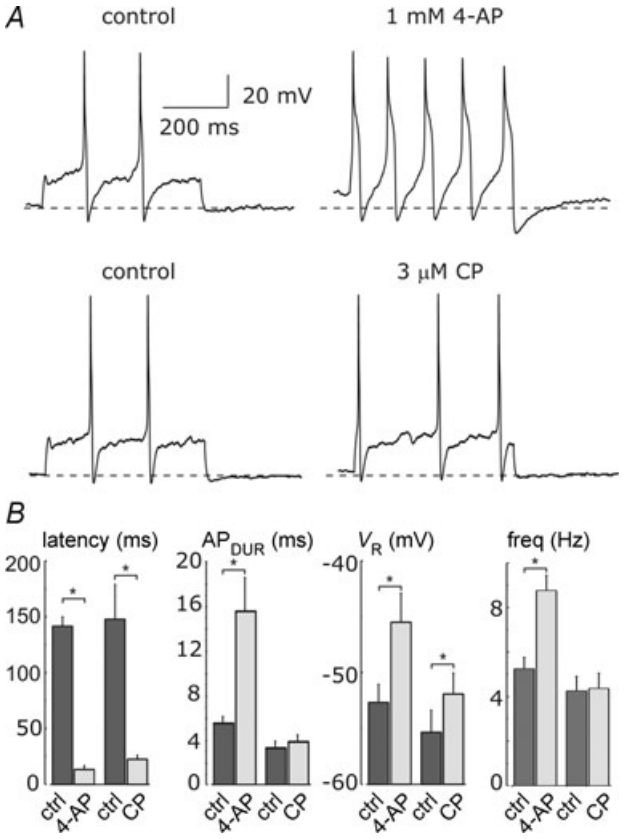

Figure 6. I_A inhibition by 4-AP and CP-339,818 eliminates the characteristic delay observed in DMF neurones
A, voltage responses to a depolarizing pulse (corresponding to the rheobase of the cells before drug application) recorded from two DMF neurones under control conditions and following bath application of 1 mM 4-AP or 3 μM CP-339,818. *B*, bar plots showing the effect of 1 mM 4-AP ($n = 6$) and 3 μM CP-339,818 ($n = 4$) on the mean first AP latency, duration of the AP at 0 mV, resting membrane potential, and firing frequency assessed from DMF neurones subject to the experimental protocol illustrated in *A*. Asterisks indicate a significant difference between values obtained under control conditions and in presence of 4-AP or CP-339,818 (*t* test, $P < 0.05$).

The DTX-sensitive current resulting from expressed Kv1 subunits is effectively inhibited by relatively low concentrations of 4-AP (Coetzee *et al.* 1999). Accordingly, we found that in large-diameter TG neurones, 100 μM and 1 mM 4-AP had an inhibitory effect resembling that found for DTX-I (Fig. 7*D* and *E*). The mean fractional block observed at −20 mV following application of 1 mM 4-AP was 0.48 ± 0.05 ($n = 5$), a value not significantly different from that observed for DTX-I (0.50 ± 0.06; $n = 7$). In addition, the normalized *I–V* relationships for the DTX- and 4-AP-sensitive currents were not appreciably different in the range −100 to −10 mV (data not shown). Finally, notice that the current remaining in the presence of DTX-I (Fig. 7*A*, middle panel), which activated with much slower kinetics, and at much higher voltages (activation threshold, *ca* −40 mV; Fig. 7*B*) resembled the high-threshold K^+ current found in small-size, I_A-negative (thus MF) neurones (see inset in Fig. 7*C*).

To clarify whether the functional expression of I_{DTX} in SS neurones is responsible for their strongly adapting firing, we looked at the effects of DTX-I on the firing response. DTX-I strongly modified the depolarization-evoked firing pattern of SS neurones, inducing a multiple-firing similar to that found in MF neurones (Fig. 8*A*). In addition, DTX-I depolarized the resting membrane potential (Fig. 8*B*) and increased slightly the duration of the action potential, although this effect did not reach statistical significance (data not shown). Similar findings were observed in SS neurones upon application of 1 mM 4-AP (data not shown).

Model results

Our experiments indicate that the selective expression of I_A and I_{DTX} in distinct subpopulations of TG neurones plays a major role in the observed diversity in

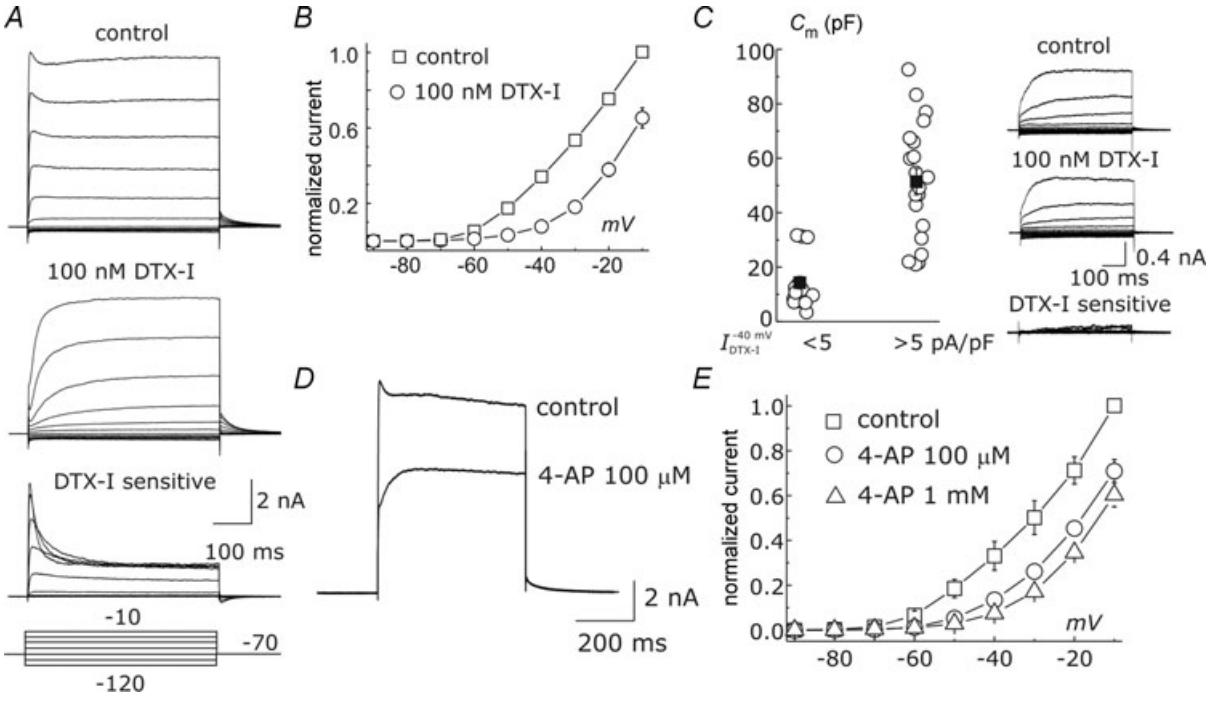

Figure 7. Properties of the low voltage threshold K^+ current expressed in SS neurones
A, current traces obtained from a large-diameter TG neurone in control conditions (upper panel) and after addition of 100 nM DTX-I (middle panel). The bottom current traces were obtained as point-by-point subtraction of the current traces in presence of DTX-I from those recorded under control conditions. Voltage-gated currents were evoked using a low-Ca^{2+}, choline-based extracellular solution (see Methods), and by applying voltage steps from −120 mV to −10 mV, in 10 mV increments, from a holding potential of −70 mV. *B*, mean, normalized *I–V* relationships obtained from 7 large-diameter TG neurones, in control conditions (□), and in presence of 100 nM DTX-I (○). The experiments used to make these plots were carried out under the same conditions described for *A*. *C*, plots of membrane capacitance of cells expressing or not expressing a detectable DTX-sensitive current (greater than 5 pA pF^{-1} at −40 mV). ○, individual TG neurones ($n = 30$), and ■, mean cell capacitances, that were found to differ significantly between neurones expressing and not expressing DTX-sensitive currents. The traces on the right are from a small TG neurone not expressing DTX-sensitive currents. *D*, current traces evoked by stepping the membrane potential from −70 mV to −20 mV in a large-diameter TG neurone in control conditions and in presence of 100 μM 4-AP. *E*, mean *I–V* relationships obtained from 5 large-diameter TG neurones under control conditions (□), in presence of 100 μM (○) and 1 mM (△) 4-AP.

the firing pattern, with the I_A being mainly responsible for the delayed multiple-firing response of DMF neurones, and the I_{DTX} for the strong firing adaptation of SS neurones. To further strengthen this conclusion, we built a mathematical model of TG neurones, and looked at the role of I_A and I_{DTX} in the simulated firing response. To this end we studied in detail the kinetic properties of I_A and I_{DTX}, and modelled them with Hodgkin–Huxley (HH) equations (Fig. 9). Specifically, the activation and inactivation kinetics of I_A were satisfactorily described with a m^3h HH model (Fig. 9*A* and *B*), where inactivation could be well described by a single exponential component up to −40 mV of applied potential. For higher depolarizations, a second, much slower inactivation time constant was needed, whose relative amplitude tended to increase at higher membrane potentials (Fig. 9*B*). The kinetic behaviour of I_{DTX} could instead be described with a m^2h HH model, incorporating a strongly voltage-dependent inactivation time constant (Fig. 9*C* and *D*). To assess the activation and inactivation parameters of I_{DTX}, we fitted the steady-state *I*–*V* relationship for the DTX-sensitive current, assessed from experiments similar to that shown in Fig. 7*A*, with a m^2h HH model. The resulting activation and inactivation $V_{½}$ values were −64 mV and −4 mV, respectively (data not shown). The mathematical model of TG neurone excitability also incorporated K^+, Na^+ and Ca^{2+} conductances typically present in TG neurones, whose properties were taken either from the literature or from our unpublished results (see Methods). The validity of the kinetic description of these currents was verified by looking at their passive and active properties resulting from the model, which we always found to fall within the range experimentally found in TG neurones.

We found a good match between the response observed in DMF neurones and that produced by the DMF neurone model built by including I_A but not I_{DTX}. A clear delay to the generation of the first AP was in fact present in the model response (Fig. 10*A*), and shown to be caused by the transient activation of I_A at the beginning of the depolarizing pulse (Fig. 10*B*). The SS neurone model, built by including I_{DTX} but not I_A, showed that the neurone was able to fire only one AP in response to depolarizing pulses, as experimentally found for SS neurones (Fig. 10*C*). Figure 10*D* shows that in response to a depolarizing pulse, the Na^+ current activates much faster than I_{DTX}, thus allowing the generation of an AP. Subsequent APs are instead prevented by the repolarizing force provided by the now active I_{DTX}. Again, in accordance with the experimental data, we found that removing I_{DTX} from the SS neurone model or reducing by one half the I_A maximal conductance in the DMF neurone model resulted in a multiple firing response typical of that found in MF neurones, together with a sensible membrane depolarization, as found in our pharmacological experiments. The DMF neurone model was also able to predict the reappearance of the delay following the injection of a hyperpolarizing continuous current able to restore the resting membrane potential observed under control conditions (full g_A), and its removal after further reducing the I_A maximal conductance (data not shown), again in accordance with our experimental data.

Discussion

Three subpopulations of mouse TG neurones with different firing patterns and functional markers

In this electrophysiological study on isolated adult mouse TG neurones we have identified three distinct neuronal subpopulations on the basis of their firing response to prolonged depolarizing currents: MF neurones, characterized by a multiple tonic firing; SS neurones, characterized by a strongly adapting

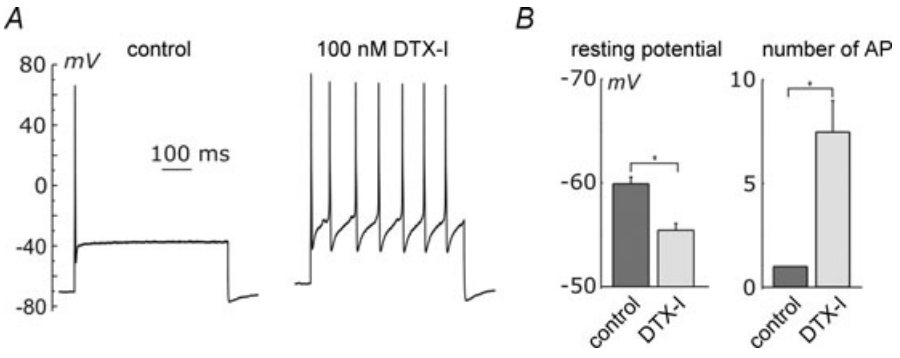

Figure 8. The DTX-sensitive current modulates the excitability of SS neurones
A, voltage traces recorded from an SS neurone in response to a depolarizing current step in control conditions (left) and in presence of 100 nM DTX-I (right). *B*, plots of the mean resting membrane potential and mean number of action potentials evoked by a 500 ms depolarizing current step at about 1.5× the rheobase of the cells before drug application, under control conditions and following application of 100 nM DTX-I ($n = 4$).

response consisting of only one AP; and DMF neurones, characterized by a delay before the beginning of repetitive firing. Notably, the DMF subpopulation had not been previously described in TG neurones. Furthermore, we have established a strong correlation between the three distinct firing patterns and other cell features such as capsaicin sensitivity, AP shape and duration that together with cell size may distinguish between neurones belonging to different functional classes.

In particular, we have shown that MF firing strongly correlates with capsaicin sensitivity, small soma and long-duration AP with typical shoulder. The strong association of some of these properties with nociceptive function (López de Armentia *et al.* 2000; Caterina & Julius, 2001; Lawson, 2002) supports the conclusion that capsaicin-sensitive MF neurones are C-type trigeminal nociceptors. The multiple firing excitability is certainly well suited to sustain the slowly adapting response seen in most C-type trigeminal nociceptors (Strassman *et al.* 1996; Levy & Strassman, 2002). DMF firing strongly correlates with capsaicin insensitivity, small soma and intermediate duration AP with typical shoulder. The functional role of DMF neurones remains uncertain. A nociceptive role also for these neurones is not to be excluded, in the light of several reports on capsaicin-insensitive nociceptors (Caterina *et al.* 1999; Nagy & Rang, 1999; Petruska *et al.* 2000; Magerl *et al.* 2001). On the other hand, low-threshold trigeminal mechanoreceptors with C-type conduction velocity have been described (Shea & Perl, 1985; Nordin, 1990). The functional significance of the delay typical of DMF neurones (due to I_A currents preventing the AP response at the beginning of the

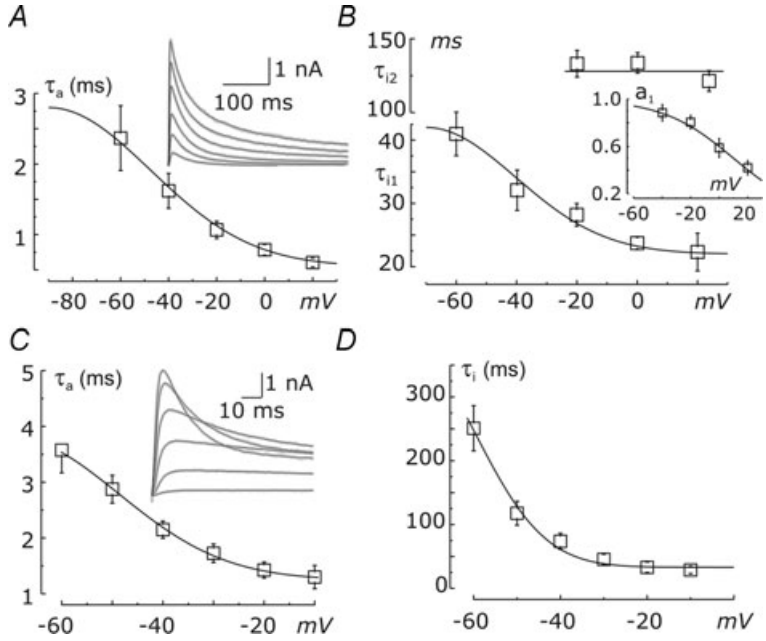

Figure 9. Kinetic properties of I_A and I_{DTX}
A, inset: I_A current traces obtained as described in Fig. 4, with superimposed the best fit with the relationship: $I_A = I_{max}\,(1 - e^{-t/\tau a})^3\,(a_1 e^{-t/\tau i1} + (1 - a_1)\,e^{-t/\tau i2})$ (in grey). The plot represents the mean τ_a–voltage relationship assessed from 4 neurones by applying the fitting procedure described in the inset. The continuous line represents the fit of the experimental data with the relationship: $\tau_a = P_1 + P_2\,\exp(-((V - P_3)/P_4)^2)$, with $P_1 = 0.55$ ms, $P_2 = 2.25$ ms, $P_3 = -90$ mV and $P_4 = 60$ mV. *B*, plot of the mean inactivation time constants as a function of voltage, assessed from 4 neurones by applying the fitting procedure described in the inset of *A*. The continuous line superimposed to the τ_{i1} data is the best fit with the relationship: $\tau_{i1} = P_1 + P_2\,\exp(-((V - P_3)/P_4)^2)$, with $P_1 = 22$ ms, $P_2 = 20$ ms, $P_3 = -70$ mV and $P_4 = 42$ mV. Inset: plot of the a_1 parameter *versus* voltage, assessed with the fitting procedure described in the inset of *A*. The continuous line represents the best fit with the relationship: $a_1 = 1/(1 + \exp((V - V_{1/2})k))$, with $V_{1/2} = 10$ mV and $k = 25$ mV. *C*, plot of the mean τ_a *versus* voltage, assessed from 5 neurones with the fitting procedure of the DTX-sensitive current as described in the inset. The continuous curve represents the best fit of the experimental data with the relationship: $\tau_a = P_1 + P_2\,\exp(-((V - P_3)/P_4)^2)$, with $P_1 = 1.25$ ms, $P_2 = 2.55$ ms, $P_3 = -70$ mV and $P_4 = 30$ mV. Inset: current trace family of DTX-sensitive currents obtained as described in Fig. 7*A*, with superimposed (in grey) the best fit with the relationship: $I_{DTX} = I_{max}\,(1 - e^{-t/\tau a})^2\,e^{-t/\tau i}$. *D*, plot of the mean τ_i *versus* voltage, assessed from 5 neurones with the fitting procedure of the DTX-sensitive current as described in *C*. The continuous curve represents the best fit of the experimental data with the relationship: $\tau_i = P_1 + P_2\,\exp(-((V - P_3)/P_4)^2)$, with $P_1 = 33$ ms, $P_2 = 339$ ms, $P_3 = -75$ mV and $P_4 = 22.2$ mV.

stimulation) could be to avoid firing following short or low-intensity stimuli. Their excitability could, however, be enhanced under inflammatory conditions, that have been shown to significantly reduce the I_A expressed in rat TG neurones (Harriot *et al.* 2006; Takeda *et al.* 2006, 2008). SS neurones differed significantly from the other two subpopulations in their larger soma size, that suggests a higher degree of myelination and conduction velocity compared to MF and DMF neurones (Lazarov, 2002). Most SS neurones were capsaicin insensitive and showed short AP duration, suggesting sensory functions other than nociception. However, a small fraction of these neurones were capsaicin responsive, and may thus represent nociceptors. Indeed, large-diameter trigeminal nociceptors (de Felipe & Belmonte, 1999; Ichikawa & Sugimoto, 2003) as well as nociceptive trigeminal sensory neurones displaying a strongly adapting response (Levy & Strassman, 2002; Takeda *et al.* 2006) have been described.

Distinct neuronal subpopulations have been previously identified in adult mouse TG neurones, based on the presence (type II neurones) or absence (type I neurones) of the Low Voltage Activated (LVA) Ca^{2+} (T-type) current (Borgland *et al.* 2001). Notable in this context, type II neurones, besides expressing T-type Ca^{2+} current, also displayed a relatively small soma size, and insensitivity to capsaicin, suggesting that they might identify with our DMF neurones. In accordance with this interpretation, our unpublished observations indicate the selective expression of an LVA Ca^{2+} current in DMF neurones. MF and SS neurones, on the other hand, appear to correspond to type I neurones, having comparable capsaicin responsiveness and more widely distributed soma size.

Ionic basis underlying the distinct firing pattern of TG neurones

We then investigated the ionic basis underlying the peculiar features of the firing of DMF and SS neurones, namely the delay to the generation of the first AP and the strong adaptation.

Preferential expression of I_A and I_{DTX} in DMF and SS neurones, respectively. Several lines of evidence indicate that a 4-AP- and CP-339,818-sensitive, fast transient I_A is

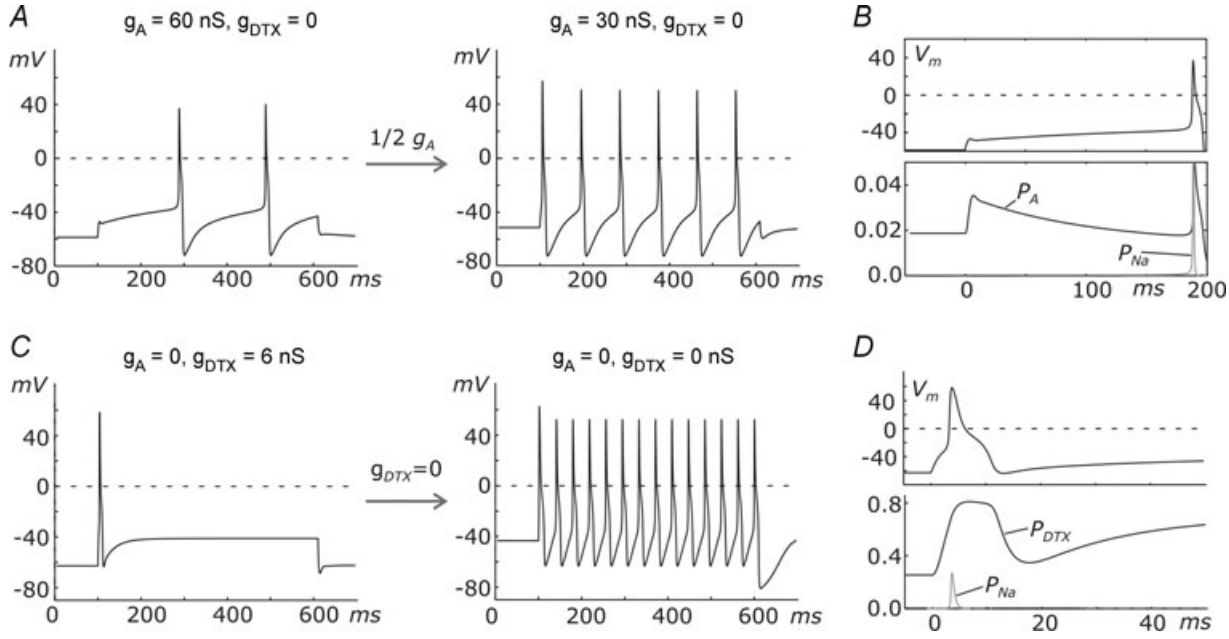

Figure 10. Modelling the role of I_A and I_{DTX} in setting the firing pattern of TG neurones
A, simulated voltage responses to a +60 pA depolarizing current pulse. The model contained an I_A with the properties experimentally found in this study, plus additional currents described in Methods. The simulation shows that the model is able to reproduce the delayed firing response typical of DMF neurones, and that reducing the I_A maximal conductance from 60 to 30 nS results in the disappearance of the delay, accompanied by a depolarization and increase in firing frequency. *B*, time course of the I_A activity Expressed in terms of open probability (P_A) and the TTX-R Na^+ current activity (P_{Na}) during the same response shown to the left of *A*. *C*, simulated voltage responses to a +200 pA depolarizing current pulse. The model contained the I_{DTX} with the properties experimentally found in this paper, plus additional currents described in Methods (the same used for the DMF neurone model of *A* and *B*). The simulation shows that the model is capable of reproducing the single-spiking response typical of SS neurones, and removing the I_{DTX} results in a depolarization and appearance of a multiple firing response. *D*, time course of the I_{DTX} activity (P_{DTX}) and the TTX-R Na^+ current activity (P_{Na}) during the same response shown in *C*, left.

preferentially expressed in DMF neurones. First, under near-physiological conditions an outward current with the biophysical and pharmacological properties of the I_A (i.e. fast inactivation, low activation voltage threshold, 4-AP sensitivity) is expressed in all DMF neurones, while it is only rarely found in the other two neuronal subpopulations. Second, under conditions that isolate K^+ currents, the I_A is selectively found in a subpopulation of neurones characterized by a cell body size and capsaicin sensitivity similar to that found for DMF neurones. Similarly, several lines of evidence indicate that I_{DTX} is preferentially expressed in SS neurones. First, under near-physiological conditions an outward current with kinetic and steady-state activation properties compatible with the presence of I_{DTX} is only found in SS neurones. Second, under conditions that isolate K^+ currents, high densities of I_{DTX} were selectively found in a subpopulation of neurones with cell body sizes selectively possessed by SS neurones. The findings discussed below support the conclusion that I_A participates in the generation of the delay to the first AP that characterizes DMF neurones, whereas I_{DTX} appears to be determinant for the strong firing adaptation typical of SS neurones.

The ionic basis of the delay in DMF neurones. Three major lines of evidence indicate that the I_A is mainly responsible for the characteristic delay preceding the first AP typical of DMF neurones. First, all DMF neurones express a considerable amount of this current. Second, blocking I_A even partially with 4-AP or CP-339,818 greatly shortened this delay (see Fig. 6). Third, a mathematical model of DMF neurones indicates that the I_A found in these neurones has properties congruent with the generation of the delay. The model also provides a detailed picture of the mechanism underlying this response: at the resting membrane potential of DMF neurones (~ -54 mV), a significant fraction of I_A is available for activation, and a portion is already activated due to the significant overlap between its activation and inactivation voltage relationships (window current; see Fig. 4). Following a depolarizing current step, this current would counteract the ensuing membrane depolarization, delaying the attainment of the voltage threshold for AP generation. At the more depolarized membrane potential established during the delay, the I_A undergoes a slow inactivation, thus allowing the membrane potential to reach the firing threshold. We finally mention that fast transient Kv currents with biophysical properties similar to those we found in TG neurones have been shown to generate such a delay in many neuronal preparations, including the functionally similar dorsal root ganglion neurones (Kanold & Manis, 1999, 2005; Shibata *et al.* 2000; Vydyanathan *et al.* 2005). However, our finding of a small fraction of MF neurones expressing I_A suggests that by itself this current may not be sufficient to cause a delayed firing response.

Currents with kinetic and steady-state activation and inactivation properties resembling those we found for I_A have been previously reported in a number of DRG and TG neuronal preparations. Of the six voltage-gated K^+ currents found in adult rat DRG neurones (Gold *et al.* 1996), our I_A has properties similar to the so-called I_{As}, with respect to both kinetics and steady-state activation and inactivation voltage range (Gold *et al.* 1996; Winkelman *et al.* 2005). A similar fast-inactivating K^+ current has also been previously described in subpopulations of rat and mouse TG neurones (Viana *et al.* 2002; Liu & Simon, 2003). Interestingly, in both TG and DRG neurones of the rat a prominent I_A has been found in capsaicin-sensitive neurones (Gold *et al.* 1996; Liu & Simon, 2003), a result that contrasts with our finding of a selective expression of this current in capsaicin-unresponsive mouse TG neurones. The different findings are probably due to species differences (mouse *versus* rat). These results are in line with recent studies showing biochemical and functional differences between mouse and rat sensory neurones (Woodbury *et al.* 2004; Price & Flores, 2007).

Fast-inactivating, A-type currents can be potentially produced by members of the *Shaker* (Kv1.4), *Shaw* (Kv3.3 and Kv3.4) and *Shal* (Kv4.1, 4.2, and 4.3) subfamilies of Kv channels. Association of Kv1 channels with certain β subunits can also originate fast-inactivating currents (Stephens *et al.* 1996). The finding that our I_A is not appreciably inhibited by DTX-I, selective blocker of Kv1.1, Kv1.2 and Kv1.6 channels, by TEA, known to fully block Kv3 subunits (Coetzee *et al.* 1999; Pérez-García *et al.* 2004), and by HpTx, a Kv4 channel-selective toxin (Sanguinetti *et al.* 1997), suggests Kv1.4 channels as a possible molecular counterpart of this current. Accordingly, we found that CP-339,818, known to selectively block Kv1.4 over the other transient K^+ channels (Nguyen *et al.* 1996), effectively blocks the I_A. Recovery from inactivation, another important feature to distinguish A-type currents produced by Kv1.4 (recovery rate, $\tau \approx 2$–4 s) from the Kv4 (recovery rate, $\tau \approx 100$ ms; Coetzee *et al.* 1999), would lead to a different conclusion. The finding that most of the I_A recovers from inactivation with fast kinetics ($\tau = 41$ ms; see Fig. 4) would in fact exclude that I_A is sustained by homomeric Kv1.4 channels, although it needs to be considered that the large number of pore-forming and accessory subunits that can concur in making up Kv channels may markedly change the biophysical and pharmacological properties of native Kv currents (Song, 2002). Further work is needed to identify conclusively the molecular nature of the I_A expressed in mouse TG neurones.

The ionic basis of the strong firing adaptation in SS neurones. Our data further show that the single-spiking response typical of SS neurones is mainly due to the expression of a DTX-sensitive, low-threshold K^+ current. This current was indeed found to be selectively expressed in a subpopulation of TG neurones characterized by a large soma size, as is the case for SS neurones. In addition, both DTX and 4-AP, blockers of I_{DTX}, were able to transform the single-spiking response of SS neurones in multiple firing. Finally, the modelling of SS neurones indicates that the low-threshold activation of I_{DTX} is able to prevent the multiple firing response. Similarly to what we found in TG neurones, DTX-sensitive currents prevent multiple firing responses in a number of neuronal preparations (Mo *et al.* 2002; Doodson *et al.* 2002; Glazebrook *et al.* 2002; Barnes-Davies *et al.* 2004). This current is indeed well suited for this role, given its particularly low voltage threshold for activation and its sustained nature at relatively low membrane potentials. Our mathematical model indicates that, following a depolarizing current pulse, the neurone can fire an AP, provided that the time elapsed has not been sufficiently long to fully activate I_{DTX}. The generation of subsequent APs will instead be prevented by the strong repolarizing force provided by the now active I_{DTX}.

As for the molecular counterpart of the I_{DTX}, a strong indication comes from the finding that this current is effectively inhibited by DTX-I, a selective inhibitor of three members of the Kv1 subfamily, Kv1.1, Kv1.2 and Kv1.6 channels (Robertson *et al.* 1996). Our data also show that I_{DTX} is fully non-inactivating only for relatively low membrane potentials. Although Kv1.1, Kv1.2 and Kv1.6 currents are all fully non-inactivating at any voltage, a strongly voltage-dependent inactivation similar to that found for I_{DTX} can be obtained when these channel subunits are co-expressed with certain β subunits, such as Kvβ1 (Stephens *et al.* 1996). It is thus possible that large-diameter TG neurones express one or more of these auxiliary subunits. In accordance with our data, immunohistochemical studies in both rat DRG and TG neurones indicate that Kv1.1 and Kv1.2 channels are preferentially expressed in medium-to-large-diameter sensory neurones (Rasband *et al.* 2001; Ichikawa & Sugimoto, 2003). Likewise several electrophysiological studies in mouse and rat DRG neurones have found low-threshold DTX-sensitive currents selectively expressed in large neurones (Pearce & Duchen, 1994; Matteson & Blaustein, 1997; Everill *et al.* 1998). DTX-sensitive currents with a more depolarized activation threshold have, however, been reported in small-diameter rat TG and DRG neurones (Beekwilder *et al.* 2003; Yoshida & Matsumoto, 2005; Gruss *et al.* 2006; Chi & Nicol, 2007).

Conclusion

In this electrophysiological study on adult mouse TG neurones, we have established a strong correlation between three neuronal subpopulations defined in terms of their firing pattern and several cell properties such as capsaicin sensitivity, AP shape and duration that together with cell size may help assign putative functional roles to the TG neurone subtypes. We have further shown that certain firing properties, namely the delay typical of DMF neurones and the strong adaptation of the SS neurones, are mainly determined by the differential expression of low-threshold voltage-gated K^+ currents: the I_A and the dendrotoxin-sensitive current, respectively. The present study, carried out on adult mouse TG neurones, gains further relevance as it represents the background for investigations in transgenic mice aimed at understanding the pathophysiological role of trigeminal sensory encoding. Particularly interesting in this respect is the investigation of possible alterations of TG neurone function in knockin mice carrying familial hemiplegic migraine mutations (van den Maagdenberg *et al.* 2004), given the key role played by activation of trigeminal meningeal nociceptors in initiation of migraine pain (Pietrobon & Striessnig, 2003).

References

Barnes-Davies M, Barker MC, Osmani F & Forsythe ID (2004). Kv1 currents mediate a gradient of principal neuron excitability across the tonotopic axis in the rat lateral superior olive. *Eur J Neurosci* **19**, 325–333.

Beekwilder JP, O'Leary ME, van den Broek LP, van Kempen GT, Ypey DL & van den Berg RJ (2003). Kv1.1 channels of dorsal root ganglion neurons are inhibited by n-butyl-p-aminobenzoate, a promising anesthetic for the treatment of chronic pain. *J Pharmacol Exp Ther* **304**, 531–538.

Bertram R & Behan M (1999). Implications of G-protein-mediated Ca^{2+} channel inhibition for neurotransmitter release and facilitation. *J Comput Neurosci* **7**, 197–211.

Borgland SL, Connor M & Christie MJ (2001). Nociceptin inhibits calcium channel currents in a subpopulation of small nociceptive trigeminal ganglion neurons in mouse. *J Physiol* **536**, 35–47.

Cabanes C, López de Armentia M, Viana F & Belmonte C (2002). Postnatal changes in membrane properties of mice trigeminal ganglion neurons. *J Neurophysiol* **87**, 2398–2407.

Caterina MJ & Julius D (2001). The vanilloid receptor: a molecular gateway to the pain pathway. *Annu Rev Neurosci* **24**, 487–517.

Caterina MJ, Rosen TA, Tominaga M, Brake AJ & Julius D (1999). A capsaicin-receptor homologue with a high threshold for noxious heat. *Nature* **398**, 436–441.

Chi XX & Nicol GD (2007). Manipulation of the potassium channel Kv1.1 and its effect on neuronal excitability in rat sensory neurons. *J Neurophysiol* **98**, 2683–2692.

Coetzee WA, Amarillo Y, Chiu J, Chow A, Lau D, McCormack T, Moreno H, Nadal MS, Ozaita A, Pountney D, Saganich M, Vega-Saenz de Miera E & Rudy B (1999). Molecular diversity of K^+ channels. *Ann N Y Acad Sci* **868**, 233–285.

Connor M, Naves LA & McCleskey EW (2005). Contrasting phenotypes of putative proprioceptive and nociceptive trigeminal neurons innervating jaw muscle in rat. *Mol Pain* **1**, 31–44.

de Felipe C & Belmonte C (1999). c-Jun expression after axotomy of corneal trigeminal ganglion neurons is dependent on the site of injury. *Eur J Neurosci* **11**, 899–906.

Dempster J (1993). *Computer Analysis of Electrophysiological Signals*. Academic Press, London.

Dodson PD, Barker MC & Forsythe ID (2002). Two heteromeric Kv1 potassium channels differentially regulate action potential firing. *J Neurosci* **22**, 6953–6961.

Everill B, Rizzo MA & Kocsis JD (1998). Morphologically identified cutaneous afferent DRG neurons express three different potassium currents in varying proportions. *J Neurophysiol* **79**, 1814–1824.

Glazebrook PA, Ramirez AN, Schild JH, Shieh CC, Doan T, Wible BA & Kunze DL (2002). Potassium channels Kv1.1, Kv1.2 and Kv1.6 influence excitability of rat visceral sensory neurons. *J Physiol* **541**, 467–482.

Gold MS, Shuster MJ & Levine JD (1996). Characterization of six voltage-gated K^+ currents in adult rat sensory neurons. *J Neurophysiol* **75**, 2629–2646.

Gruss M, Ettorre G, Stehr AJ, Henrich M, Hempelmann G & Scholz A (2006). Moderate hypoxia influences excitability and blocks dendrotoxin sensitive K^+ currents in rat primary sensory neurones. *Mol Pain* **2**, 12–26.

Gutman GA, Chandy KG, Grissmer S, Lazdunski M, McKinnon D, Pardo LA, Robertson GA, Rudy B, Sanguinetti MC, Stühmer W & Wang X (2005). International Union of Pharmacology. LIII. Nomenclature and molecular relationships of voltage-gated potassium channels. *Pharmacol Rev* **57**, 473–508.

Harriott AM, Dessem D & Gold MS (2006). Inflammation increases the excitability of masseter muscle afferents. *Neuroscience* **141**, 433–442.

Harvey AL & Robertson B (2004). Dendrotoxins: structure-activity relationships and effects on potassium ion channels. *Curr Med Chem* **11**, 3065–3072.

Herzog RI, Cummins TR & Waxman SG (2001). Persistent TTX-resistant Na^+ current affects resting potential and response to depolarization in simulated spinal sensory neurons. *J Neurophysiol* **86**, 1351–1364.

Ichikawa H & Sugimoto T (2003). Kv1.2-immunoreactive primary sensory neurons in the rat trigeminal ganglion. *Brain Res* **974**, 222–227.

Kanold PO & Manis PB (1999). Transient potassium currents regulate the discharge patterns of dorsal cochlear nucleus pyramidal cells. *J Neurosci* **19**, 2195–2208.

Kanold PO & Manis PB (2005). Encoding the timing of inhibitory inputs. *J Neurophysiol* **93**, 2887–2897.

Lawson JJ, McIlwrath SL, Woodbury CJ, Davis BM & Koerber HR (2008). TRPV1 unlike TRPV2 is restricted to a subset of mechanically insensitive cutaneous nociceptors responding to heat. *J Pain* **9**, 298–308.

Lawson SN (2002). Phenotype and function of somatic primary afferent nociceptive neurones with C-, Aδ- or Aα/β-fibres. *Exp Physiol* **87**, 239–244.

Lazarov NE (2002). Comparative analysis of the chemical neuroanatomy of the mammalian trigeminal ganglion and mesencephalic trigeminal nucleus. *Prog Neurobiol* **66**, 19–59.

Levy D & Strassman AM (2002). Mechanical response properties of A and C primary afferent neurons innervating the rat intracranial dura. *J Neurophysiol* **88**, 3021–3031.

Liu L, Oortgiesen M, Li L & Simon SA (2001). Capsaicin inhibits activation of voltage-gated sodium currents in capsaicin-sensitive trigeminal ganglion neurons. *J Neurophysiol* **85**, 745–758.

Liu L & Simon SA (1996). Similarities and differences in the currents activated by capsaicin, piperine, and zingerone in rat trigeminal ganglion cells. *J Neurophysiol* **76**, 1858–1869.

Liu L & Simon SA (2003). Modulation of I_A currents by capsaicin in rat trigeminal ganglion neurons. *J Neurophysiol* **89**, 1387–1401.

López de Armentia M, Cabanes C & Belmonte C (2000). Electrophysiological properties of identified trigeminal ganglion neurons innervating the cornea of the mouse. *Neuroscience* **101**, 1109–1115.

Magerl W, Fuchs PN, Meyer RA & Treede RD (2001). Roles of capsaicin-insensitive nociceptors in cutaneous pain and secondary hyperalgesia. *Brain* **124**, 1754–1764.

Matteson DR & Blaustein MP (1997). Scorpion toxin block of the early K^+ current (IKf) in rat dorsal root ganglion neurones. *J Physiol* **503**, 285–301.

Mo ZL, Adamson CL & Davis RL (2002). Dendrotoxin-sensitive K^+ currents contribute to accommodation in murine spiral ganglion neurons. *J Physiol* **542**, 763–778.

Nagy I & Rang HP (1999). Similarities and differences between the responses of rat sensory neurons to noxious heat and capsaicin. *J Neurosci* **19**, 10647–10655.

Nguyen A, Kath JC, Hanson DC, Biggers MS, Canniff PC, Donovan CB, Mather RJ, Bruns MJ, Rauer H, Aiyar J, Lepple-Wienhues A, Gutman GA, Grissmer S, Cahalan MD & Chandy KG (1996). Novel nonpeptide agents potently block the C-type inactivated conformation of Kv1.3 and suppress T cell activation. *Mol Pharmacol* **50**, 1672–1679.

Nordin M (1990). Low-threshold mechanoreceptive and nociceptive units with unmyelinated (C) fibres in the human supraorbital nerve. *J Physiol* **426**, 229–240.

Pearce RJ & Duchen MR (1994). Differential expression of membrane currents in dissociated mouse primary sensory neurons. *Neuroscience* **63**, 1041–1056.

Pérez-García MT, Colinas O, Miguel-Velado E, Moreno-Domínguez A & López-López JR (2004). Characterization of the Kv channels of mouse carotid body chemoreceptor cells and their role in oxygen sensing. *J Physiol* **557**, 457–471.

Petruska JC, Napaporn J, Johnson RD, Gu JG & Cooper BY (2000). Subclassified acutely dissociated cells of rat DRG: histochemistry and patterns of capsaicin-, proton-, and ATP-activated currents. *J Neurophysiol* **84**, 2365–2379.

Pietrobon D & Striessnig J (2003). Neurobiology of migraine. *Nat Rev Neurosci* **4**, 386–398.

Price TJ & Flores CM (2007). Critical evaluation of the colocalization between calcitonin gene-related peptide, substance P, transient receptor potential vanilloid subfamily type 1 immunoreactivities, and isolectin B4 binding in primary afferent neurons of the rat and mouse. *J Pain* **8**, 263–272.

Rasband MN, Park EW, Vanderah TW, Lai J, Porreca F & Trimmer JS (2001). Distinct potassium channels on pain-sensing neurons. *Proc Natl Acad Sci U S A* **98**, 13373–13378.

Robertson B, Owen D, Stow J, Butler C & Newland C (1996). Novel effects of dendrotoxin homologues on subtypes of mammalian Kv1 potassium channels expressed in Xenopus oocytes. *FEBS Lett* **383**, 26–30.

Sanguinetti MC, Johnson JH, Hammerland LG, Kelbaugh PR, Volkmann RA, Saccomano NA & Mueller AL (1997). Heteropodatoxins: peptides isolated from spider venom that block Kv4.2 potassium channels. *Mol Pharmacol* **51**, 491–498.

Shea VK & Perl ER (1985). Sensory receptors with unmyelinated (C) fibers innervating the skin of the rabbit's ear. *J Neurophysiol* **54**, 491–501.

Shibata R, Nakahira K, Shibasaki K, Wakazono Y, Imoto K & Ikenaka K (2000). A-type K^+ current mediated by the Kv4 channel regulates the generation of action potential in developing cerebellar granule cells. *J Neurosci* **20**, 4145–4155.

Song WJ (2002). Genes responsible for native depolarization-activated K^+ currents in neurons. *Neurosci Res* **42**, 7–14.

Stephens GJ, Cockett MI, Nawoschik SP, Schecter LE & Owen DG (1996). The modulation of the rate of inactivation of the mKv1.1 K^+ channel by the beta subunit, Kv beta 1 and lack of effect of a Kv beta 1 N-terminal peptide. *FEBS Lett* **378**, 250–252.

Strassman AM, Raymond SA & Burstein R (1996). Sensitization of meningeal sensory neurons and the origin of headaches. *Nature* **384**, 560–564.

Takeda M, Tanimoto T, Ikeda M, Nasu M, Kadoi J, Yoshida S & Matsumoto S (2006). Enhanced excitability of rat trigeminal root ganglion neurons via decrease in A-type potassium currents following temporomandibular joint inflammation. *Neuroscience* **138**, 621–630.

Takeda M, Tanimoto T, Nasu M & Matsumoto S (2008). Temporomandibular joint inflammation decreases the voltage-gated K^+ channel subtype 1.4-immunoreactivity of trigeminal ganglion neurons in rats. *Eur J Pain* **12**, 189–195.

van den Maagdenberg AM, Pietrobon D, Pizzorusso T, Kaja S, Broos LA, Cesetti T, van de Ven RC, Tottene A, van der Kaa J, Plomp JJ, Frants RR & Ferrari MD (2004). A Cacna1a knockin migraine mouse model with increased susceptibility to cortical spreading depression. *Neuron* **41**, 701–710.

Viana F, de la Peña E & Belmonte C (2002). Specificity of cold thermotransduction is determined by differential ionic channel expression. *Nat Neurosci* **5**, 254–260.

Vydyanathan A, Wu ZZ, Chen SR & Pan HL (2005). A-type voltage-gated K^+ currents influence firing properties of isolectin B4-positive but not isolectin B4-negative primary sensory neurons. *J Neurophysiol* **93**, 3401–3409.

Winkelman DL, Beck CL, Ypey DL & O'Leary ME (2005). Inhibition of the A-type K^+ channels of dorsal root ganglion neurons by the long-duration anesthetic butamben. *J Pharmacol Exp Ther* **314**, 1177–1186.

Woodbury CJ, Zwick M, Wang S, Lawson JJ, Caterina MJ, Koltzenburg M, Albers KM, Koerber HR & Davis BM (2004). Nociceptors lacking TRPV1 and TRPV2 have normal heat responses. *J Neurosci* **24**, 6410–6415.

Yoshida S & Matsumoto S (2005). Effects of alpha-dendrotoxin on K^+ currents and action potentials in tetrodotoxin-resistant adult rat trigeminal ganglion neurons. *J Pharmacol Exp Ther* **314**, 437–445.

Yoshida S, Takahashi M, Kadoi J, Kitagawa J, Saiki C, Takeda M & Matsumoto S (2007). The functional difference between transient and sustained K^+ currents on the action potentials in tetrodotoxin-resistant adult rat trigeminal ganglion neurons. *Brain Res* **1152**, 64–74.

Zarayskiy VV, Balasubramanian G, Bondarenko VE & Morales MJ (2005). Heteropoda toxin 2 is a gating modifier toxin specific for voltage-gated K^+ channels of the Kv4 family. *Toxicon* **45**, 431–442.

Acknowledgements

This work was supported by Italian Ministry of University (Prin 2005, to D.P.), and Telethon-Italy (Grant GGP06234, to D.P.)